



HAL
open science

Investigation of growth limitation by CO₂ mass transfer and inorganic carbon source for the microalga *Chlorella vulgaris* in a dedicated photobioreactor

Benjamin B. Le Gouic, H. Marec, J. Pruvost, J.F. F Cornet

► To cite this version:

Benjamin B. Le Gouic, H. Marec, J. Pruvost, J.F. F Cornet. Investigation of growth limitation by CO₂ mass transfer and inorganic carbon source for the microalga *Chlorella vulgaris* in a dedicated photobioreactor. *Chemical Engineering Science*, 2021, 233, pp.116388. 10.1016/j.ces.2020.116388 . hal-03474428

HAL Id: hal-03474428

<https://uca.hal.science/hal-03474428>

Submitted on 3 Feb 2023

HAL is a multi-disciplinary open access archive for the deposit and dissemination of scientific research documents, whether they are published or not. The documents may come from teaching and research institutions in France or abroad, or from public or private research centers.

L'archive ouverte pluridisciplinaire **HAL**, est destinée au dépôt et à la diffusion de documents scientifiques de niveau recherche, publiés ou non, émanant des établissements d'enseignement et de recherche français ou étrangers, des laboratoires publics ou privés.



Distributed under a Creative Commons Attribution - NonCommercial 4.0 International License

**INVESTIGATION OF GROWTH LIMITATION BY CO₂ MASS
TRANSFER AND INORGANIC CARBON SOURCE FOR THE
MICROALGA *CHLORELLA VULGARIS* IN A DEDICATED
PHOTOBIOREACTOR**

B. Le Gouic¹, H. Marec¹, J. Pruvost*¹, J.F. Cornet²

¹ Université de Nantes, ONIRIS, CNRS, GEPEA, UMR 6144, F-44600, France

² Université Clermont Auvergne, CNRS, SIGMA Clermont, Institut Pascal, F-63000 Clermont-
Ferrand, France

* Author to whom correspondence should be addressed

Telephone: (33) (0)2 40 17 26 69

Fax: (33) (0)2 40 17 26 18

e-mail: jeremy.pruvost@univ-nantes.fr

Abstract

An experiment was set up using a well-controlled photobioreactor to characterize the CO₂ transfer and assimilation by photosynthetic microorganisms. This lab-scale system enabled accurate monitoring of the carbon sources in liquid and gas phases for in-depth characterization of the CO₂ physical transfer and biological consumption of dissolved carbon.

This paper presents a validation of the set-up by assessing the carbon mass balance in various absorption/desorption experiments. This is represented by the Carbon Recovery Percentage, which was found to be equal to 1 ± 0.1 confirming the accuracy of the time monitoring for the various carbon fluxes. These carbon fluxes were modeled to determine on-line the gas-liquid mass transfer coefficient (k_{LA}). This enabled investigation of some aspects of CO₂ dissolution in water, such as the effect of the culture medium composition and its pH value. Finally, carbon assimilation and growth limitation by the carbon source were studied for the microalga *Chlorella vulgaris*.

Keywords: photobioreactor, microalgae, CO₂ transfer, gas-liquid mass transfer; biofixation, modelling, *Chlorella vulgaris*

1 Introduction

The rise of global atmospheric CO₂ since the industrial revolution is mainly due to CO₂ emissions from the combustion of fossil fuels, gas flaring and cement production. Measurements of NOAA (Mauna Loa station) show that CO₂ concentration in the atmosphere rose from 350 ppm in 1990 to 407 ppm in 2016. The average rate of increase in carbon dioxide concentration over the period 1960 to 2005 is 1.4 ppm/yr (Solomon et al., 2007). Global warming, climate changes observed in different areas and ocean acidification (Rice and Herman, 2012) are some examples of the effects of carbon dioxide that directly impact the Earth. Solutions must be found to mitigate the carbon footprint of human activity.

Carbon capture technologies already exist for treating the CO₂ emitted by plants, by means of post-combustion, pre-combustion or oxy-combustion capture devices (Kanniche et al., 2010), for example. Captured carbon can then be stored to prevent its release into atmosphere. This is mainly applied in depleted oil and gas fields and saline aquifers, although the safety and reliability of the approach for long-term storage is still uncertain (Luis et al., 2012). This, combined with the investment needed and/or the energy costs of the processes needed for CO₂ capture, now makes the generalization of these solutions mandatory for CO₂ emitting industries.

Biological valorization of CO₂ appears to be another solution of interest. This can be achieved through mass microalgae and cyanobacteria culture (Huntley and Redalje, 2007), since these photosynthetic microorganisms have the ability to use inorganic carbon to synthesize organic carbon compounds as they grow. In optimized systems, they also grow faster than higher plants and are able to fix more CO₂ per unit of land area than terrestrial plants. Biomass, or its valuable components such as pigments, proteins and fatty acids, can therefore potentially be used for application in various fields such as food and biofuels (Carlsson et al., 2007; Pulz and Gross, 2004), enabling development of a waste-to-value approach in which flue gas can be converted into biomass, which can be economically exploited.

Photosynthetic microorganisms such as microalgae contain approximately 50% molecular carbon per kg of dry weight (DW) of biomass, and the theoretical fixed quantity of carbon is 1.83 kg CO₂ per kg DW. In terms of kinetics, biomass productivity has to be as high as possible in order to maximize CO₂ fixation via the Calvin cycle. This implies investigation of different aspects to fully

exploit the ability of microalgae for optimal assimilation of CO₂. In a general way, biomass needs non-limited access to all growth nutrients in order to avoid limitation or starvation, which can seriously impact the growth rate, and consequently the CO₂ fixation rate, of the culture. This concerns nutrients like nitrogen, phosphorus and sulfur sources (i.e. nitrate, ammonium, phosphate and sulfate), but also the carbon source itself. To be assimilated by photosynthetic microorganisms, gaseous CO₂ must first be transferred to the liquid phase to form dissolved inorganic carbon (DIC). Once dissolved, pH-dependent reactions dissociate inorganic carbon into three different chemical species: CO_{2,d}, HCO₃⁻ and CO₃²⁻. Of these, only dissolved carbon dioxide (CO_{2,d}) and bicarbonate (HCO₃⁻) are assimilated by cells.

The diffusion coefficient of carbon dioxide in water is around 10,000-fold lower than in air. Consequently, the carbon injection in culture systems, and therefore its mass transfer, must be taken into account so that the carbon requirement for biomass growth is not underrated. The other consequence is that full CO₂ dissolution or consumption of injected CO₂ is rarely achieved in culture systems. The theoretical stoichiometric requirement of 1.83 kg CO₂ per kg of dry biomass would therefore appear difficult to achieve in practice. For example, Doucha *et al.* (Doucha *et al.*, 2005) report an effective requirement of 4.4 kg CO₂/kg DW taking into account the massive loss of carbon which occurs in the open culture systems used by these authors.

The difference between the theoretical and effective requirements necessarily indicates the relevance in understanding and modelling the gas-liquid mass transfer and HCO₃⁻ consumption rates in the cultivation system. To optimize carbon use by the microalgal culture, the volumetric gas-liquid mass transfer coefficient $k_{L}a$ should therefore ideally be known, and this depends greatly on conditions for the experiment such as gas and liquid phases mixing, pH, temperature, and liquid phase composition. The concentration of total dissolved inorganic carbon is also especially relevant, as it fixes the quantity available for biomass growth and also the driving force for mass transfer (i.e. the difference in CO₂ concentration between gas and liquid phases). A direct comparison can be made here with the well-known issues relating to oxygen dissolution in heterotrophic culture systems (i.e. bacteria, yeasts). Recent studies, however, have reported lower overall carbon dioxide mass-transfer coefficients compared to those obtained with oxygen (Hill, 2006; Kordac and Linek, 2008). Typically, the mass transfer coefficient for CO₂ ($k_{L}a$) is estimated using the mass transfer coefficient for O₂ then

combined with the correlation, taking into account the diffusion coefficients of both CO₂ and O₂ (Royce and Thornhill, 1991). This can lead to some inconsistency, however, due to the difference of dissolution chemistry between CO₂ and O₂.

In addition to the gas-liquid mass transfer efficiency of the process, the effect of DIC on growth should also be known, ideally, as it drives the biological assimilation of injected CO₂. Due to the low CO₂ concentration in the atmosphere (around 0.04%), photosynthetic microorganisms in natural growth conditions frequently suffer from carbon limitation. They have therefore developed several mechanisms to reduce the effects of growth limitation by the carbon source, usually referred as carbon concentration mechanisms (CCM). For low carbon concentration, the diffusion of carbon dioxide or active transport of bicarbonate through the cell membrane (Price et al., 1998), combined with the low activity of carbonic anhydrase, is insufficient for optimal fixation by photosynthesis. The intracellular concentration mechanisms of inorganic carbon, implying dedicated carbon transporters of both CO₂ and HCO₃⁻, are consequently induced to concentrate carbon in the vicinity of Rubisco ((Giordano et al., 2005). This enables enough carbon to be provided for the carboxylase reaction, leading to sugar generation via the Calvin cycle (Badger and Price, 2003; Spalding, 2008). For example, in cyanobacteria, active transport mechanisms allow the cells to reach an internal bicarbonate concentration of around 20-40 mmol L⁻¹ for external concentration of dissolved inorganic carbon as low as 0.02 mmol L⁻¹ (Price and Howitt, 2011).

However, carbon source active transporters are energy-consuming mechanisms and therefore have a negative effect on growth rates. Baba and Shiraiwa (Baba and Shiraiwa, 2012) have shown that the specific growth rate for *Chlamydomonas reinhardtii* decreases gradually at under 1% (vol.) of CO₂ in air (no indication of DIC concentration provided). Multiple acclimation states are also described for *Chlamydomonas reinhardtii*, depending on carbon concentration in the medium. For CO₂ concentrations up to 0.5% in air (vol.), no limiting-CO₂-inducible gene is expressed, whereas for concentrations under 0.01% and between 0.03-0.4%, the induction of limiting-CO₂-regulated genes was observed, associated with a marked decrease in photosynthetic growth rate (Spalding, 2008). We note also that all these mechanisms are reversible, as they disappear when carbon reaches a sufficient concentration in the growing environment. Acclimation between two extreme conditions typically occurs within a few hours (Miyachi et al., 2003).

All previous studies confirm that once a sufficient DIC is maintained in the medium, no growth limitation by the carbon source occurs, so the biomass productivity is driven by other operating factors, such as light energy transfer rate (Pruvost et al., 2012). Carbon assimilation is therefore stoichiometrically related to growth rate, so in this regard, optimization of carbon biofixation in culture systems can be considered a trivial task. This requires attainment of only a sufficient non-limiting DIC value by bubbling-in the medium air enriched in CO₂, or by bicarbonate enrichment of the growing medium. However, due to the effect of carbon dissolution on pH, special attention must be paid to keeping the resulting pH value within the optimal range for the species being cultivated (this is easy to achieve by control strategy with CO₂ injection only without constraint on the CO₂ mole fraction in the output of the gas phase). It should be noted, however, that if the purpose is to optimize carbon supply to the culture (i.e. minimization of the CO₂ needed for a given biomass production, or maximization of CO₂ dissolution efficiency in the liquid phase), the increase in driving force will benefit from gas dissolution as this will increase the carbon mass transfer from the gas to the liquid phase. For any CO₂ concentration in the gas phase, the maximum driving force will be obtained for the minimum value of DIC. As a result, the optimization of both carbon fixation (related to growth, which indicates that a minimal DIC must be reached to avoid growth limitation) and CO₂ dissolution from the gas phase (related to gas-liquid mass transfer, which indicates ideally a null DIC) is contradictory. This implies that the underlying physical, biological and chemical mechanisms must be characterized, and ideally modeled, for their respective optimization.

The aim of this study is to develop an experiment set-up for investigating and modeling carbon dioxide fixation by microalgae in the well-controlled conditions of a lab-scale photobioreactor. By combining liquid and gaseous analyses, the carbon fluxes were validated from mass balance, and the gas-liquid mass transfer $k_L a$ was determined. This was used to establish a mass transfer model considered as microalgae biological assimilation. The model was then used for in-depth analysis of various carbon fluxes occurring during the process between biomass (CO₂ biofixation), gaseous (loss of CO₂) and liquid phases (accumulation of dissolved inorganic carbon) as a function of the operating conditions (pH, CO₂ concentration in gas inlet, DIC in growing medium). Finally, effects of growth limitation by the carbon source are investigated in both batch and continuous culture.

2 Materials and methods

2.1 Microorganism and medium

Chlorella vulgaris (2111/19 CCAP) was retained as a case-study and cultivated in an autotrophic medium based on Sueoka medium with the following composition: NH_4Cl ; 27.1 mM, $\text{MgSO}_4 \cdot 7\text{H}_2\text{O}$; 1.14 mM, $\text{CaCl}_2 \cdot 2\text{H}_2\text{O}$; 0.34 mM, K_2HPO_4 ; 4.48 mM and 1 mL/L of Hutner solution growth medium. For the PBR cultivation, pH and temperature were controlled at 7.5 and 25 °C respectively. Pure water was used in the various experiments and for medium preparation (Millipore Elix System, United States).

2.2 Lab-scale pilot

The set-up for the experiment is shown in Figure 1. The lab-scale CO_2 pilot was based on a 1.5 L torus-shaped photobioreactor (PBR), described elsewhere (Degrenne, 2009; Fouchard et al., 2008; Martzloff et al., 2012; Pottier et al., 2005). This culture system was designed for rigorous control of all growing conditions such as light, mixing, pH and temperature. It can be operated in batch or continuous mode. The culture was mechanically stirred by a marine impeller, which also provided accurate analysis of the gas phase in the PBR outlet, as demonstrated in the case of hydrogen production by microalgae (Degrenne, 2009). The alternative airlift systems which are commonly used in the field require a minimum gas flow rate for good mixing performance. This leads to dilution of the gas produced or consumed by biological reaction. Due to the mechanical mixing, gas dilution remains limited in the torus-shaped PBR, thereby greatly increasing the accuracy in determining the concentration of gas produced or consumed by the culture. This advantage was extended (i) in this study, to investigate CO_2 fixation by microalgae with dedicated development, therefore, of the monitoring and control of the gas phase, and (ii) in pH acid/base regulation, to disconnect CO_2 dissolution from pH evolution; pH and DIC being closely related.

Flow meters/controllers were used in the gas inlet and outlet of the PBR (El-Flow[®] select, Bronkhorst[®] High tech, Germany). These were controlled by proprietary software (Flow DDE, Bronkhorst[®] High tech, Germany). In the PBR inlet, flow meters/controllers were connected to N_2 and

CO₂ bottles to produce gas mixture with different CO₂ enrichment, by setting the N₂ and CO₂ mass flow meters at the relevant proportions.

The pressure inside the PBR was measured (Sensortech; 0-5 bar, Germany) and maintained constant at atmospheric pressure by using a needle valve. For safety reasons, this was done with a solenoid valve that was allowed to open in the event of excessive pressure. Gas in the outflow was passed through a condenser and a drying tube (Drierite®) to suppress humidity, and finally brought to the CO₂ analyzer (SIEMENS Ultramat 6E). For a high level of accuracy in the mass balance at the gas phase, the analyzer was used in differential mode and the difference in CO₂ concentration between gas inlet and outlet measured (Δy_{CO_2} in ppm). This analyzer was equipped with a non-dispersive infra-red detector (NDIR) with a range of Δy_{CO_2} measurements from 0 to 5000 ppm of CO₂.

The PBR was placed on a weighing scale (Mettler Toledo, New classic ML, Switzerland) enabling on-line monitoring. When the weight variation surpassed 2 grams, a peristaltic pump (Ismatec, Reglo Digital) was activated to remove the excess culture medium with a pipe directly immersed in the liquid phase. This overflow system allows gas analysis even in continuous culture mode (not used in this study) by preventing part of the gas from being lost in the outlet when used for culture harvest (as can be obtained by applying a culture overflow). Note that this also increases the accuracy of the analysis by keeping the liquid volume (and therefore the gas hold-up) constant throughout all the experiments.

Except where mentioned, a constant total gas flow rate of 100 mL/min was imposed in the PBR inlet in all studies, but with different CO₂ enrichment. The marine impeller was set at 250 rpm to ensure homogenization of the liquid phase.

Temperature and pH were monitored (sensor Mettler Toledo Inpro 3253i, Switzerland). Temperature was controlled by automatic air blowing from a fan (air-conditioned room), and pH was regulated by hydrochloric acid or soda-lime injections (Stepdos pump 03/RC, KNF Neuberger, Germany) depending on the operating conditions.

2.3 Analyses

2.3.1 Biomass dry weight concentration and elementary analysis

A known volume of algal suspension depending on biomass concentration was filtered through a dried filter weighed beforehand (Wathman GF/F, 0.7 μm). All minerals in the growth medium were filtered out by washing the biomass with distilled water. The filter was then dried at 110°C for 24 h before being weighed again to determine the biomass concentration.

For elementary analysis, biomass samples were concentrated by centrifugation (6 min at 3600 g) and lyophilized. Elementary analysis was performed by the CNRS Central Analysis Service (Vernaison, France).

2.3.2 Pigment content

Each analysis was done in triplicate. Pigment content was extracted with methanol. A volume of culture depending on biomass concentration was introduced with a 2 mL Eppendorf tube and centrifuged at 12100 g for 5 minutes. The supernatant was discarded and the pellet suspended in 1.5 mL of methanol. The three tubes were incubated for 1 h at 45 °C and centrifuged in the same conditions as before. The supernatant was then analyzed with a spectrophotometer (Perkin Elmer, Lambda 2S). Chlorophyll a (Chl-a), chlorophyll b (Chl-b) and photoprotective carotenoid (PPC) were determined according to Ritchie (Ritchie, 2008, 2006) for chlorophylls and Strickland and Parsons (Strickland and Parsons, 1968) for carotenoids:

$$[Chl - a] \text{ mg/L} = [-8.0962 \cdot (A_{652} - A_{750}) + 16.5169 \cdot (A_{665} - A_{750})] \cdot V_2 \cdot L^{-1} \cdot V_1^{-1} \quad \mathbf{1)}$$

$$[Chl - b] \text{ mg/L} = [27.4405 \cdot (A_{652} - A_{750}) - 12.1688 \cdot (A_{665} - A_{750})] \cdot V_2 \times L^{-1} \cdot V_1^{-1} \quad \mathbf{2)}$$

$$[PPC] \text{ mg/L} = [4 \cdot (A_{480} - A_{750})] \cdot V_2 \times L^{-1} \cdot V_1^{-1} \quad \mathbf{(3)}$$

2.3.3 Liquid phase analysis

The dissolved inorganic carbon (DIC) was measured with a TOC meter (TOC5000A, Shimadzu, Japan). The carrier gas (oxygen Alphagaz 1 quality, Air Liquide, France) was used at a

flow rate of 150 mL/min for degassing DIC in phosphoric acid (25% w/w). CO₂ was then carried in an NDIR detector to determine the inorganic carbon concentration (mg/L, then converted into mol/L). Dilutions of a 1 g/L DIC standard (NaHCO₃ = 0.35 g/L dried on silica gel and Na₂CO₃ = 0.445 g/L dried 1 hr at 285 °C) were used for calibration. Each data sample corresponded to an average of 3 measurements.

For experiments with microalgae culture, samples were filtered beforehand to remove biomass (Minisart 0.2 µm, Sartorius, Germany).

2.3.4 Gas phase analysis

To determine the carbon transferred to the photobioreactor (PBR), measurements of the gaseous phase concentration in both the inlet and the outlet of the PBR were taken, denoted $y_{CO_2}^i$ and $y_{CO_2}^o$ respectively. This was obtained by a CO₂ gas analyzer (SIEMENS Ultramat 6E, Germany) working in differential mode (see above for how it was integrated in the experiment set-up).

2.3.5 Calculation of carbon recovery percentage

The carbon recovery percentage (CRP) represents the accuracy of the carbon mass balance onto the PBR. This is an effective way of confirming the overall set-up for the experiment (PBR and analysis of all carbon sources). The carbon feed to the lab-scale CO₂ pilot in either gas (CO₂) or liquid (HCO₃⁻) form has to be recovered in the liquid phase (where it can be assimilated by microalgae) or in the gas outlet. Complete analysis and monitoring of phase composition therefore provides information on the carbon assimilation by microalgae, and also on the CO₂ mass transfer between phases.

The CRP is based on calculation of the ratio between carbon transferred in the liquid phase and carbon evolution in the gaseous phase between the PBR inlet and outlet. Because this ratio evolves with time, it is calculated for all points i (N points) in the experiment, obtained in the process monitoring:

$$CRP = \frac{\sum_{i=1}^N \left(\frac{(C_T^i - C_T^{i-1}) \cdot V_L}{\frac{(\Delta y_{CO_2}^i + \Delta y_{CO_2}^{i-1})}{2} \cdot G \cdot (t_i - t_{i-1})} \right)}{N} \quad (4)$$

Similarly, the CO₂ removal ratio can be determined from analysis of the gas phase (Cheng et al., 2006):

$$\eta = \frac{y_{CO_2}^i - y_{CO_2}^o}{y_{CO_2}^i} \quad (5)$$

This value allows the percentage of carbon transferred in the PBR to be quantified for biomass synthesis or accumulation in the liquid phase.

3 Theoretical considerations

3.1 Gas dissolution

The thermodynamic equilibrium of CO₂ between the gas phase and the liquid phase is given by Henry's law (Henry, 1803), which relates the concentration of dissolved carbon dioxide ($C_{CO_2,L}$) to the partial pressure of gaseous CO₂ (p_{CO_2}):

$$p_{CO_2} = H_{CO_2} \cdot C_{CO_2,d} \quad (6)$$

with Henry's constant H depending on temperature, as defined for example by (Edwards et al., 1975):

$$\ln(H) = -\frac{6789.04}{T} - 11.4519 \cdot \ln(T) + 94.4914 \quad (7)$$

Henry's law fixes the maximum concentration of dissolved CO₂ that can be achieved for a given partial pressure of CO₂: p_{CO_2} , as in the following equation, and can be modified by increasing the total pressure P_r , or increasing the molar fraction of CO₂ in the gas y_{CO_2} :

$$p_{CO_2} = y_{CO_2} \cdot P_r \quad (8)$$

Henry's law is valid for a dilute solution with moderate temperature and pressure, and a fugacity coefficient equal to 1, which is the case with most aeration conditions in photosynthetic cultures (Cornet et al., 1998). Additionally, the CO₂ solubility may be affected (Henry's constant increases) by ionic dissolved species; nevertheless, in this study, considering the low electrolytes concentration in the culture medium, we will assume a deviation for the Henry's constant less than 10% and finally work with its value in pure water.

3.2 Carbon dissociation in the liquid phase

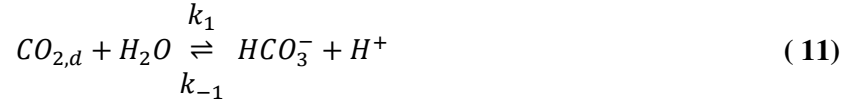
CO₂ is a weak acid which dissociates, in basic conditions, into bicarbonate and carbonate ions. A first chemical equilibrium involves dissolved carbon dioxide (CO_{2,d}) and carbonic acid (H₂CO₃) as:



Carbonic acid then dissociates into bicarbonate ion:



Reactions (9) and (10) can be combined to obtain the following reaction:



Bicarbonate ion dissociates then into carbonate ion:



Each reaction has a dissociation equilibrium constant defined as:

$$K_1 = \frac{C_{HCO_3^-} \cdot C_{H^+}}{C_{CO_{2,L}} \cdot C_{H_2O}} = \frac{k_1}{k_{-1}} \quad (13)$$

$$K_2 = \frac{C_{CO_3^{2-}} \cdot C_{H^+}}{C_{HCO_3^-}} = \frac{k_2}{k_{-2}} \quad (14)$$

Note that, for the same reasons as discussed above on the CO₂ solubility, we assumed in this study that the concentrations in dissolved species of the culture medium were sufficiently low to enable working with ideal solution assumption on the liquid phase. The dissociation equilibrium constants K₁ and K₂ are given by Edwards (1978) as a function of temperature (K) in moles of solutes per kilogram of water:

$$\ln(K_1) = -\frac{12092.1}{T} - 36.7816 \cdot \ln(T) + 235.482 \quad (13)$$

$$\ln(K_2) = -\frac{12431.7}{T} - 35.4819 \cdot \ln(T) + 220.067 \quad (14)$$

The concentration C_T of dissolved inorganic carbon (DIC) is given as the sum of all carbon species in the liquid phase:

$$C_T = C_{CO_{2,L}} + C_{HCO_3^-} + C_{CO_3^{2-}} \quad (15)$$

By combining this equation with the constant for dissociation of each carbon species, the DIC concentration can be expressed as a function of the pH and $CO_{2,L}$:

$$C_T = K \cdot C_{CO_{2,L}} \quad (16)$$

with:

$$K = 1 + \frac{K_1}{C_{H^+}} + \frac{K_1 \cdot K_2}{C_{H^+}^2}$$

We can note that carbon chemistry allows the concentration attainable at equilibrium to be determined (all these chemical reactions are very fast compared to the characteristic time constants of the process), but not the transfer kinetics, which must be obtained from the mass balances for both gas and liquid phases (see paragraph below).

3.3 Mass balance

3.3.1 Mass balance in the liquid phase

In the liquid phase, the carbon mass balance is related to the carbon chemistry and therefore to the different carbon species, as obtained from the pH-value dependent dissociation (see paragraph above). Because of the high mixing efficiency of the torus-shaped PBR (Pruvost et al., 2006), the liquid phase was considered to be well mixed. Considering that the liquid phase was kept in the PBR (batch culture), the carbon mass balance for each dissolved carbon species concentration was therefore:

$$\left\{ \begin{array}{l} \frac{dC_{CO_{2,L}}}{dt} = a \cdot N_{CO_2} - k_1 \cdot C_{CO_{2,L}} + k_{-1} \cdot C_{HCO_3^-} \cdot C_{H^+} \\ \frac{dC_{HCO_3^-}}{dt} = k_1 \cdot C_{CO_{2,L}} + k_{-2} \cdot C_{CO_3^{2-}} \cdot C_{H^+} - k_{-1} \cdot C_{HCO_3^-} \cdot C_{H^+} - k_2 \cdot C_{HCO_3^-} \\ \frac{dC_{CO_3^{2-}}}{dt} = k_2 \cdot C_{HCO_3^-} - k_{-2} \cdot C_{CO_3^{2-}} \cdot C_{H^+} \end{array} \right. \quad (17)$$

with a the exchange interfacial area per unit of culture volume (m^{-1}), and N_{CO_2} the carbon molar flux density between liquid and gaseous phases ($mole \cdot m^{-2} \cdot s^{-1}$).

Since we consider the equilibrium between various carbon species to be set quasi-instantaneously ($\frac{dC_{HCO_3^-}}{dt} = \frac{dC_{CO_3^{2-}}}{dt} = 0$), we can assume that the system of Eqs.(19) can be simplified as:

$$\begin{cases} \frac{dC_{CO_2,L}}{dt} = \frac{1}{K} \cdot a \cdot N_{CO_2} \\ C_{HCO_3^-} = \frac{K_1 \cdot C_{CO_2,L}}{C_{H^+}} \\ C_{CO_3^{2-}} = \frac{K_2 \cdot C_{HCO_3^-}}{C_{H^+}} \end{cases} \quad (18)$$

Note that following Eq. 18, the carbon molar flux can finally be defined as a function of the DIC (C_T):

$$\frac{dC_T}{dt} = a \cdot N_{CO_2} \quad (21)$$

3.3.2 Mass balance in the gaseous phase

As the PBR is continuously stripped by a constant gas molar flow rate G , the gaseous phase was considered as an open system. A mass balance on the gas phase therefore leads to:

$$V_G \cdot \frac{dC_{CO_2,g}}{dt} = -a \cdot V_L \cdot N_{CO_2} + y_{CO_2}^i \cdot G_i - y_{CO_2}^o \cdot G_o \quad (22)$$

Assuming gaseous CO_2 to be an ideal gas, the above expression can be expressed as:

$$\frac{P \cdot V_G}{R \cdot T} \cdot \frac{dy_{CO_2}}{dt} = -a \cdot V_L \cdot N_{CO_2} + y_{CO_2}^i \cdot G_i - y_{CO_2}^o \cdot G_o \quad (19)$$

As the gas phase is continuously stripped, CO_2 accumulation in the gas phase can be disregarded (André et al., 1981) and a quasi steady state can be assumed:

$$a \cdot N_{CO_2} = \frac{1}{V_L} \cdot (y_{CO_2}^i \cdot G_i - y_{CO_2}^o \cdot G_o) \quad (20)$$

By assuming a negligible transfer of the gas carrier (N_2) to the liquid phase, the N_2 molar flow rate (G) can be considered constant between the PBR inlet and outlet. This allows the related inlet (G_i) and outlet flow rate (G_o) and their respective molar fractions:

$$G = G_i \cdot (1 - y_{CO_2}^i) = G_o \cdot (1 - y_{CO_2}^o) \quad (21)$$

Finally, because the CO₂ molar fraction in the gas phase (between 4.10⁻⁴ and 1.10⁻²) and the mass transfer intensity are low, the total molar flow rate can also be considered constant between the PBR inlet and outlet:

$$G_i \cong G_o \cong G \quad (22)$$

This gives the final expression of the mass balance for the gaseous phase as:

$$a \cdot N_{CO_2} = \frac{G}{V_L} \cdot \Delta y_{CO_2} \quad (23)$$

$$\text{where } \Delta y_{CO_2} = y_{CO_2}^i - y_{CO_2}^o \quad (24)$$

Note that following Eq.27 and 28, the measurement of the difference Δy_{CO_2} in molar fraction of CO₂ in gas phase between the PBR inlet and outlet enables the carbon transferred ($a \cdot N_{CO_2}$) to be determined between the phases for a given molar flow rate G and volume V_L in the liquid phase.

3.4 Gas-liquid mass transfer

Gas-liquid mass transfer is the phenomenon which occurs when the liquid and gas phases are not at a thermodynamic equilibrium. The molar flux density N between the two phases can therefore be represented by:

$$N = k \cdot \Delta C \quad (25)$$

where k is the mass transfer coefficient and ΔC is a the concentration difference, usually called the potential or driving force for mass transfer.

The bi-layer mass transfer model is particularly adapted to the case of gas-liquid mass transfer (Lewis and Whitman, 1924). It enables mass transfer resistance to be located in either the gas or liquid boundary layer. For a gas with poor solubility, such as CO₂, the mass transfer resistance is located in the liquid phase. The mass transfer coefficient (denoted k_L) is then related to the liquid phase. By introducing the specific area available for mass transfer (denoted a), the mass transfer equation for CO₂ becomes:

$$a \cdot N_{CO_2} = k_{L,CO_2} \cdot a \cdot \Delta C_{CO_2,d} \quad (26)$$

where $\Delta C_{CO_2,d}$ is the driving force for CO₂ dissolution in the liquid phase which may be expressed differently, depending of the model retained for the ideal flow of the gas phase (see the following section).

3.5 Determination of overall volumetric mass transfer coefficient ($k_L a$)

The overall volumetric carbon dioxide mass transfer coefficient (denoted $k_L a$) depends on definition of the driving force. By definition, this driving force expresses the mass transfer potential between phases and is therefore a function of the difference between the carbon concentration in current phases and that obtained at mass transfer equilibrium. This leads to different possible formulations of the driving force.

Assuming first a perfectly mixed gas phase in the photobioreactor leads to retain for the CO_2 saturation concentration at equilibrium the value $C^* = \frac{y_{\text{CO}_2}^o P}{H}$. In some cases, the mass transfer rate is very low and the input and output mole fractions are closed enabling to choose $C^* = \frac{y_{\text{CO}_2}^i P}{H}$ which has the advantage to uncouple the liquid mass balance from the gas mass balance. In these two cases (well-mixed gas phase), the volumetric mass transfer term is written easily:

$$a \cdot N_{\text{CO}_2} = k_L a \cdot \left(C^* - \frac{C_T}{K} \right) \quad (31)$$

Finally, the more accurate assumption is to consider the gas phase with a plug flow model leading to a more complex form of the volumetric mass transfer rate ($a N_{\text{CO}_2}$) (Roustan, 2003).

All these possibilities in writing the term ($a N_{\text{CO}_2}$) are then summarized in Table 1. In the remaining part of this study, the three possible values of identified volumetric mass transfer coefficient were named respectively: $k_L a^{y_{\text{CO}_2}^o}$, $k_L a^{y_{\text{CO}_2}^i}$ and $k_L a^{PF}$.

4 Results

4.1 Investigation of carbon absorption/desorption in pure water and culture medium

4.1.1 Experimental determination of the overall carbon dioxide mass transfer coefficient

Several carbon absorption/desorption experiments were conducted to validate the set-up. For absorption experiments, gas enriched with CO_2 was continuously injected at a given flowrate and composition in the torus PBR, which was filled with a liquid phase with null initial DIC. For desorption experiments, the liquid phase was first enriched with dissolved carbon by adding a given

amount of bicarbonate, and a CO₂-free gas phase was injected (pure N₂). The progressive enrichment/depletion of the liquid phase in DIC was monitored as well as the evolution in CO₂ concentration in the gas outlet. Absorption and desorption experiments were carried out for both pure water and culture growth medium (coalescent and non-coalescent medium) to investigate whether minerals contained in the growth medium could affect mass transfer by, for example, affecting bubble size and thereby the interfacial exchange surface.

For all experiments, pH and temperature were regulated respectively at 7.5 and 25 °C. This regulation was necessary to fix the carbon chemistry in the liquid phase. Values were chosen to correspond to optimal growth conditions for *Chlorella vulgaris* (the same conditions were applied in subsequent batch cultures). For all experiments, the carbon recovery percentage (CRP) was calculated from time evolutions of the carbon content measured in the gas and liquid phases. This was found to be a relevant criterion as a value of 1 imposed on the PBR was perfectly tight and all analytical devices were accurately calibrated. All experiments were found to be valid if CRP was equal to 1 ± 0.1 .

A typical CO₂ desorption result is given in Figure 2. Time monitoring of both liquid (Fig.2-a) and gas (Fig.2-b) phases enabled determination of the gas-liquid mass transfer coefficient $k_{L,a}$ for each experiment. Fig.2-c gives the Carbon Recovery Percentage (CRP), which was found to be close to 1 ± 0.1 throughout the experiment. Fig.2-d presents analysis of the data used to calculate $k_{L,a}$ values. Depending on the definition of the driving force, different slopes and therefore $k_{L,a}$ values were obtained, as explained in section 3.3.2. This emphasizes the relevance of an accurate definition of the driving force when measuring the gas-liquid mass transfer coefficient $k_{L,a}$ (not always clear in the literature). All results are summarized in Table 2.

The $k_{L,a}$ value was found to be dependent on the operating conditions (whatever the definition of the driving force). For example, $k_{L,a}$ in desorption was found to be higher in culture medium than in pure water, as explained definitively by the decrease in bubble size resulting in an increase of salt-enriched medium in the interfacial area (in the range 30-50%, depending on driving force definition). Note that this result was observed previously by Loubiere et al. (Loubiere et al., 2011). More surprisingly, the $k_{L,a}$ value was found to be different in absorption and desorption experiments, at around 20% and 30% for pure water and growth medium respectively. These results were also

observed previously (Kordac and Linek, 2008) and could be attributable to the particular carbon chemistry of the liquids.

Because different k_{LA} values were observed for the various conditions investigated, the corresponding k_{LA} value was used for each case in the rest of the study. Note that this value is usually obtained and then fixed from specific preliminary investigations into conditions which are different most of the time from the ones applied (different medium, presence of microalgal cells, etc.). This can lead to a possible bias when relating growth rate to gas-liquid mass transfer. In our set-up, we were able to deduce the k_{LA} value directly from the data monitored for each experiment. Because this value is relevant for accurate modeling of the carbon mass transfer, direct measurement of the k_{LA} value is clearly of interest for an accurate representation of various carbon fluxes in the process, as was subsequently carried out.

4.1.2 Validation of carbon mass transfer model

4.1.2.1 *CO₂ absorption in pH-regulated conditions*

Two experiments were conducted to validate the accuracy of the mass transfer model, in order to predict the evolution of carbon concentration in the gas and liquid phases. In the first experiment, a CO₂ pulse was applied in pure water. Note that this is often used in practice with a carbon supply to microalgae culture when applying pH-regulated injection.

For the first four hours of the experiment, the carbon concentration in the gas injection was 1700 ppm, then increased to 4800 ppm. Time evolutions of the gas composition and DIC concentration are given in Figure 3. The experimental data were compared to model predictions with k_{LA} values determined from previous sections for absorption in pure water (2.6 h⁻¹ for the plug flow model). Model predictions are given in the form of envelopes, by introducing the possible deviation of experimental operating parameters (i.e. ± 0.1 , $\pm 10^{-4}$ and $\pm 0.2\text{h}^{-1}$ for pH, $y_{CO_2}^i$ and k_{LA} values respectively) to the input parameters of the model. Errors are summarized in Table 3 for all definitions of the driving force used in the mass transfer model.

The highest discrepancy between experiment and model prediction was obtained just after the CO₂ pulse. This could be attributable to the sudden change in operating conditions. Nevertheless, experimental evolutions were found to be comprised in envelope prediction, emphasizing the accuracy

of our model prediction. The greatest error was found in the prediction of outlet gas composition $y_{CO_2}^o$ (maximum error around 7%, based here on the average data of the envelope prediction). For DIC concentration, which is the most relevant data for this study, the relative error was kept below 4%.

4.1.2.2 Dissolved carbon desorption without pH regulation

The second experiment consisted of dissolved carbon desorption with no pH regulation of the liquid phase, to evaluate the ability of the model to represent the relation between dissolved carbon chemistry and pH value. Due to carbon desorption, a progressive decrease in carbonated ion concentration was obtained, resulting in a progressive basification of the liquid phase due to the decrease in H^+ concentration, in respect of the electroneutrality principle (i.e. $\sum z_i C_{\text{cations}} = \sum z_j C_{\text{anions}}$).

The liquid phase (pure water) was initially enriched with DIC (7.5 mM) and a constant gas flowrate composed of pure nitrogen was then applied ($6L \cdot h^{-1}$) for 25 hours. The DIC concentration of the liquid phase and gas composition were monitored. Results are given in Figure 4. The progressive desorption of inorganic carbon can easily be seen, resulting in an increase in pH value. The highest CO_2 content in the gas phase was obtained at the beginning of the experiment as a result of the higher driving force due to the high initial concentration of DIC. After 25 hours, only low gas desorption was observed (low CO_2 content in the outlet gas phase). This is explained by the lower driving force between the liquid and gas phases, and also by the higher pH value ($pH > 9$) which is favorable to carbon dissolution. As a result, total desorption was not achieved at the end of the experiment. Although a progressive decrease in DIC concentration was obtained, the liquid phase was still enriched with dissolved carbon after 25 hrs of N_2 bubbling, indicating a very low desorption rate.

Prediction results for the carbon mass transfer model are added in Figure 4. A constant k_{La} value of $2.6h^{-1}$ as achieved in the section above was applied (desorption in pure water, plug flow model). To model the pH evolution, a mass balance equation based on the water electroneutrality principle at quasi steady-state was added in the model, which indicated that the concentration of cationic compounds was equal to that for the anionic ones (i.e. $\sum z_i C_{\text{cations}} = \sum z_j C_{\text{anions}}$). As a result, the H^+ concentration and therefore pH value (i.e. $pH = -\log(C_{H^+})$) were related to the concentration of carbonated ions (Eq.18).

As with the CO₂ pulse absorption experiment, an accurate prediction of the time evolutions of gas composition and DIC concentration was obtained (relative error of 10% for DIC concentration). The liquid phase basification was also predicted but with less accuracy: a slight underestimation of around 0.2 unit in pH value is observed as commonly encountered in the literature. . For values higher than pH 8, a slight variation in pH results in a wide variation in DIC concentration. This could make it challenging to accurately determine the k_{LA} values from mass balance onto the culture volume, as applied previously. k_{LA} values determined at neutral pH were therefore used for the rest of the study (Table 3).

4.2 Investigation of carbon assimilation during *Chlorella vulgaris* growth in PBR

4.2.1 Description of experiments

Three *Chlorella vulgaris* cultures were carried out under different molar fractions of CO₂ in the inlet of the gas phase, which were obtained by mixing CO₂ with nitrogen gas. Values were chosen from literature to investigate growth rate with and without limitation by the carbon source. In Experiment 1 (E1), the CO₂ enrichment in the nitrogen gas phase was set at 2200 ppm. According to Spalding (Spalding, 2008), this should correspond to low limitation of the growth by the carbon source. In Experiment 2 (E2), the CO₂ enrichment was increased to 6500 ppm, which is above the carbon limited condition presented by Spalding (2008). The incident photons flux density (PFD) was set at $250 \mu\text{mol}_{\text{hy}} \cdot \text{m}^{-2} \cdot \text{s}^{-1}$ in both cases. To investigate the role of light, which influences the growth rate of biomass and therefore its carbon requirement, it was finally decided to define another case study (E3), which was conducted under an incident PFD of $400 \mu\text{mol}_{\text{hy}} \cdot \text{m}^{-2} \cdot \text{s}^{-1}$ with a nitrogen gas enriched in 7700 ppm in CO₂. For all experiments, nutrients (except DIC) were provided in large amounts to avoid growth limitation. Biomass and DIC concentrations were measured daily so as not to disturb the culture.

4.2.2 Modification of mass balance equations

The mass balance equations used for model predictions were modified to take into account the biological consumption of CO₂ by microalgae as photosynthetic growth rate ($\langle r_{CO_2} \rangle$):

$$\frac{dC_T}{dt} = a \cdot N_{CO_2} - \langle r_{CO_2} \rangle \quad (32)$$

By introducing the mass balance on the gas phase that remains unchanged (Eq.25), we can write:

$$\frac{dC_T}{dt} = \frac{G}{V_L} \cdot (y_{CO_2}^i - y_{CO_2}^o) - \langle r_{CO_2} \rangle = \frac{G}{V_L} \cdot \Delta y_{CO_2} - \langle r_{CO_2} \rangle \quad (33)$$

Note that simultaneous monitoring of the gas (Δy_{CO_2}) and liquid phases (C_T) allows direct determination of the molar volumetric biological consumption rate of CO₂ ($\langle r_{CO_2} \rangle$, here expressed in moles). As a result, if the volumetric productivity of the biomass (i.e. biomass growth rate) is also measured from the dry-weight concentration ($\langle r'_X \rangle = \frac{dC_X}{dt}$, here expressed in mass), the mass yield of biological consumption of CO₂ (in kg CO₂/kg dry mass) can be deduced from experimental data:

$$Y_{CO_2} = \frac{\langle r_{CO_2} \rangle \cdot M_{CO_2}}{\langle r'_X \rangle} \quad (34)$$

with M_{CO_2} the molar mass of CO₂.

4.2.3 Experimental investigation of the impact of carbon limitation on *Chlorella vulgaris* growth

Figure 5 presents *Chlorella vulgaris* growth for experiments E1 and E2. An almost linear increase in biomass concentration was obtained in both cases, allowing the corresponding biomass growth rates to be determined. Throughout the experiments, compositions in the gas and liquid phase were almost constant, indicating a constant gas-liquid mass transfer (Eq.27). Table 4 gives the corresponding time averaged values.

Biomass growth rate $\langle r'_X \rangle$ was found to increase with the molar fraction of CO₂ in the gas injection. This was directly correlated to the increase of CO₂ transferred to the liquid phase (N_{CO_2} ; note that N_{CO_2} is proportional to Δy_{CO_2} due to the constant gas flowrate, Eq.27). In experiment E2, the growth rate observed was 3 times higher than in experiment E1. Regarding DIC concentration (C_T), a lower value was measured in E1, but it should be noted that both experiments led to low DIC concentrations of under 0.1mM. These low concentrations could indicate an insufficient carbon supply due to insufficient gas-liquid mass transfer, most of the transferred carbon therefore being assimilated by the biomass growth.

To confirm whether a possible carbon limitation occurs, it was decided to increase the CO₂ content in the gas phase to a molar fraction of 7700 ppm (Experiment E3). To eliminate the risk of growth limitation by the light supply, the incident PFD was also increased to 400 μmol_{hv} · m⁻² · s⁻¹. An increase of biomass productivity was obtained (Table 4). The biomass productivity increase was again found to be directly related to the increase in CO₂ fixation (N_{CO₂}), but considering the increase in incident PFD, a higher increase in biomass productivity was expected (about 9-10%), indicating possible limitation by the carbon supply, although DIC concentration was increased to about 0.4 mM.

Despite its strong influence on growth kinetics, the CO₂ supply was found to have a negligible effect on the biomass elemental composition, which was found to be similar for all studies with a carbon, nitrogen and phosphorus content of respectively around 48%, 8.9% and 0.9%. Based on this composition, the theoretical yield of CO₂ assimilation per unit of biomass and biomass molar weight can be determined (Pruvost et al., 2009), leading to Y_{CO₂}=1.76 kg CO₂ per kg DW and M_X = 24 g/mol_c. These values will be used in the section below to analyze carbon fluxes. We can note here that the yield of CO₂ assimilation is similar to values reported in the literature (1.83 kg CO₂ per kg DW (Chisti, 2007)).

Finally, Table 4 presents the influence of the CO₂ supply on biomass pigment content. For constant PFD (250 μmol_{hv} · m⁻² · s⁻¹), the pigment content was found to decrease as carbon limitation increased, with a total pigment content of 4.7% and 6.1% for E1 and E2 respectively. A lower pigment content was observed at 400 μmol_{hv} · m⁻² · s⁻¹, but this could be attributable to the greater amount of light received per cell, which is also known to induce photoacclimation and therefore a decrease in pigment content (Souliès et al., 2016a). Our results tend therefore to emphasize that pigment acclimation is also influenced by carbon uptake.

4.2.4 Analysis of carbon fluxes during *Chlorella vulgaris* culture

The aim of this study was not to optimize the carbon fixation rates in *Chlorella vulgaris* culture. As a first asset of the interest of the experimental set-up, however, we estimated the CO₂ removal ratio η , representing the percentage of carbon transferred in the photobioreactor for biomass synthesis or accumulation in the liquid phase. This can be obtained from Table 4, using previous eq. (5):

$$\eta = \frac{y_{CO_2}^i - y_{CO_2}^o}{y_{CO_2}^i} = \frac{\Delta y_{CO_2}}{y_{CO_2}^i} \quad (35)$$

For all experiments, CO₂ removal was found to be in the range 45-50%, even though low DIC concentrations were obtained (significant driving force for gas-liquid mass transfer). In the context of using microalgae to reduce CO₂ emission from an industrial flue gas, this demonstrates that it would be challenging to achieve a high rate of CO₂ removal. Gas-liquid mass transfer of the cultivation systems would be especially relevant for that purpose (see Eq.27 and 30).

Complete monitoring of both gas and liquid phases enabled a more in-depth analysis of the carbon fluxes involved during microalgae growth. As a first remarkable result, if the biomass molar weight is used to determine biomass productivity on a C-mol basis (Table 4), we can observe that the carbon flux for gas-liquid mass transfer $\langle r_{CO_2} \rangle$ is very close to the biomass growth rate when both values are expressed on a C-mol basis. As a consequence of the mass balance, dissolved carbon accumulation in the liquid phase therefore remains negligible, as confirmed by our analysis ($C_T < 0.4$ mM).

Based on this, Eqs.32-33 can be simplified and the biological CO₂ consumption estimated directly from gas analysis (i.e. $\frac{G}{V_L} \cdot \Delta y_{CO_2} = \langle r_{CO_2} \rangle = a N_{CO_2}$). This allows the yield of biological CO₂ consumption Y_{CO_2} from Eq.34 to be determined for each experiment. Values close to the theoretical values reported in literature were obtained (1.83 for Chisti 2007, 1.76 as deduced from our elementary composition analysis), namely 1.77, 1.96 and 2.00 for experiments E1, E2 and E3 respectively. The slight increase from experiments E1 to E3 could be attributable to the simplification hypothesis applied in Eq.33, which disregards the accumulation of dissolved carbon when calculating the biological consumption of CO₂ (as shown in Table 4, DIC concentration increases from E1 to E3). It could also be attributable to the production of exo-metabolites, which are not measured in biomass productivity calculation (dry-weight measurement). This can be improved easily for future experiments by time-monitoring of dissolved organic and inorganic carbon concentrations. Despite this, our results indicate that there is no significant change in the biological CO₂ consumption yield. Such result was expected because, a constant carbon content (i.e. close to 50%) also indicates a constant CO₂ consumption yield (around 1.8). This illustrates here carbon concentration mechanisms (CCM), which reduce limitation effects by the carbon source on the metabolism. A decrease in growth

rate was obtained (i.e. almost proportional to the carbon gas-liquid mass transfer), but with no significant impact on the biological CO₂ consumption yield and then biomass carbon content.

Following Eq.27 and 31, the gas-liquid mass transfer coefficient $k_L a$ can also be determined from on-line measurements:

$$a \cdot N_{CO_2} = k_L a \cdot \left(C^* - \frac{c_T}{K} \right) = \frac{G}{V_L} \cdot (y_{CO_2}^i - y_{CO_2}^o) \quad (36)$$

$$\text{and then} \quad k_L a = \frac{G}{V_L} \cdot \frac{(y_{CO_2}^i - y_{CO_2}^o)}{\left(C^* - \frac{c_T}{K} \right)} \quad (37)$$

A constant value of $3.75 \pm 0.04 \text{ h}^{-1}$ was obtained for the three experiments (values here obtained with the plug flow model). This can be attributed to the accurate control of mixing conditions in the torus-shaped PBR (Pruvost et al., 2006) which, combined with accurate control of the injected gas flow rate (constant here), led us to maintain similar gas-liquid mass transfer conditions for all experiments. This guarantees accurate investigation of the carbon feeding on the resulting microalgal growth. However, it can be noted that the $k_L a$ values obtained in *Chlorella vulgaris* cultures were higher than those measured with only culture medium (2.1 h^{-1} , Table 2). This could be attributable to a modification of gas phase characteristics, such as interfacial area (i.e. bubble size) by microalgal cells. This again emphasizes the interest of on-line determination of the gas-liquid mass transfer coefficient, which was possible with our experiment set-up. The use of data obtained from measurements without the biological phase (as is usually done in practice) would have led to errors in carbon flux analysis. By enabling redundant information, our experiment set-up enabled direct measurement of $k_L a$ for each new experiment, and therefore a detailed and accurate analysis of all carbon fluxes involved in the process.

4.3 Investigation of carbon assimilation during *Chlorella vulgaris* growth in PBR

4.3.1 Description of experiments

The limitation of growth by the carbon source has been studied more in depth by conducting continuous culture under constant PFD of $200 \mu\text{mole} \cdot \text{m}^{-2} \cdot \text{s}^{-1}$ and with permanent feeding in culture medium at a given constant residence time τ_p . Only CO₂ enrichment of the gas phase was modified, as given in Table 5. Five CO₂ concentration in the gas injection were tested ranging from 400ppm (i.e.

atmospheric CO₂ content, Case 1) to pure CO₂ (Case 5). Please note however that the last concentration was not compatible with the limit of the CO₂ analyzer, Case 5 being retained here to obtain a reference value with growth only limited by light. Pure CO₂ injection were then controlled by pH regulation, as described elsewhere for investigations of the light-limited growth (Souliès et al., 2016b). For all experiments, the PBR was operated with a constant inlet total gas flowrate of 100mL.min⁻¹. The N₂ gas injection was then modified accordingly, to take into account of the change in CO₂ content.

Only steady-state results were here considered but it has to be noticed that in some cases, steady-state establishment took a long time before to be obtained. This was especially the case when shifting from conditions leading to high DIC concentration in the culture medium to ones leading to significant DIC decrease (see later for DIC values). The daily monitoring of the DIC concentration revealed that several days (up to 20 days) were necessary to stabilize DIC concentration. For conditions leading to growth limitation by DIC concentration (Cases 1 to 4), this directly affected the growth kinetics and then resulting biomass concentration, which in turns modified light attenuation conditions and then resulting growth kinetics. As a global result, culture steady-state were found longer to obtain as in the typical cases where only light limitation occurs (i.e. typically between 3 to 6-fold the residence time τ_p applied on the culture system, corresponding to around 3 to 6 days of continuous operation). Please note that such behavior, which is related to the DIC concentration and so gas-liquid mass transfer performance of the PBR, could explain in practice some apparent instability in PBR operation as it typically results in oscillations with time of the biomass concentration during the time necessary to achieve constant DIC concentration and light attenuation conditions.

4.3.2 Effects of carbon limitation on *C.vulgaris* growth

Figure 6 shows *C. vulgaris* biomass concentration and corresponding volumetric productivity obtained at steady-state for the various conditions investigated. As expected, higher concentrations and productivities were obtained for Case 5 corresponding to growth limitation by light only. The typical curve of a continuous culture with a progressive decrease in biomass concentration with the increase in dilution rate was obtained ((Takache et al., 2012) This reduced the effect of light attenuation in the

PBR bulk, resulting in an increase in biomass productivity up to a peak value of around $1.6 \cdot 10^{-2} \text{kg} \cdot \text{m}^{-3} \cdot \text{h}^{-1}$. This maximal productivity was then obtained for an optimal residence time ($\tau_p=25.6\text{h}$), also corresponding to an optimal biomass concentration (i.e. around $C_x=0.42\text{kg} \cdot \text{m}^{-3}$) leading to optimal light attenuation conditions in the culture volume (i.e. luminostat regime corresponding to full light absorption with no dark zone in the culture bulk).

For all other cases, the progressive decrease in CO_2 content in the gas phase resulted in a decrease in biomass concentration and productivity. For Case 1, corresponding to the atmospheric CO_2 content (i.e. air bubbling), a significant decrease was obtained with productivity around $6 \cdot 10^{-4} \text{kg} \cdot \text{m}^{-3} \cdot \text{h}^{-1}$ indicating a severe growth limitation. As a consequence, only large residence time values were permitted ($\tau_p=200\text{h}$).

Analysis of biochemical composition revealed that only pigment contents were strongly affected by the carbon limitation, as in batch mode (the content in proteins, sugar and lipids were found indeed similar whatever the condition ; data not shown). Pigment content decreases from 7% to 2% between Case 5 (no carbon limitation) and Case 1 (lower CO_2 content).

In fact, this is difficult to disconnect the respective influence of carbon limitation and light attenuation conditions, as both CO_2 gas composition but also residence times were varied in our experiments (i.e. residence time only is known to strongly influence light attenuation conditions which also influence pigment content). We can notice however that experiments conducted with a similar residence time $\tau_p=71.4\text{h}$ (i.e. Cases 2, 3 and 5) clearly emphasizes the effect of carbon limitation. Decreasing the CO_2 content to 2200ppm (Case 2) results to a decrease of pigment content down to 4% (7% for Case 5 without limitation). But this also corresponds to a significantly lower biomass concentration, with $0.34\text{kg} \cdot \text{m}^{-3}$ and $0.99\text{kg} \cdot \text{m}^{-3}$ for Case 2 and 5 respectively. This lower biomass concentration results in a higher rate of light absorption per cell, which is known to induce photoacclimation and pigment decrease (Kandilian et al., 2016; Souliès et al., 2016c). Those authors obtained similar values (i.e. 2%) in low biomass concentration but without carbon limitation.

We also observed that the distribution between various pigments (Chla, Chlb and photoprotective carotenoids) stayed almost constant whatever the conditions investigated: $69 \pm 3\%$ chlorophyll a, $15 \pm 2\%$ chlorophyll b and $14 \pm 2\%$ photoprotective carotenoids (values relative to total pigment content). A change is usually related to a nutrient growth limitation which is known to induce

a high increase in the carotenoids to chlorophylls ratio. So our finding on a stable pigment composition is in accordance with the rather stable biochemical composition obtained in terms of proteins-sugar-lipids contents. So, those results tends to indicate that the carbon limitation mainly affects growth kinetics and, as a result, that the pigment decrease is an indirect effect of carbon limitation. By reducing the growth kinetics, a lower biomass concentration is achieved for a given operating condition (i.e. residence time), resulting in a lower light attenuation and then higher rate of photons absorption, which finally leads to a lower pigment content due to cells photoacclimation.

To emphasize limitation of growth kinetics by the carbon source, biomass productivities were expressed as a function of the maximal biomass productivity obtained without carbon limitation (Case 5, noted $\langle r'_x \rangle_{\text{photolimitation}}$). Because of the influence of dilution rate on biomass productivity, only maximal productivities for each case were considered (i.e. values estimated from Fig.6 for cases C2, C3, C4 and C5, noted $\langle r'_x \rangle_{\text{max}}$ in Table 5). In all cases, a complete monitoring of the carbon composition in both gas and liquid phases was conducted. This allowed determining DIC and the variation of CO_2 $\Delta y_{\text{CO}_2} = y_{\text{CO}_2}^l - y_{\text{CO}_2}^o$ in the gas composition between PBR inlet and outlet (except for C5 which presented a CO_2 content in the gas phase out the gas analyzer range). Results were added to Table 5.

A direct relation between growth kinetics (i.e. biomass productivity) with the CO_2 content in the feeding gas phase is clearly emphasized. For the lower CO_2 content (Case 1, atmospheric CO_2 content), the maximal biomass productivity is only around 4% of the values achieved without carbon limitation (Case 5). For intermediate values, a progressive decrease is observed. We can note that Case 4 presents maximal productivities close to the one achieved without carbon limitation (i.e. 98%). This indicates that a minimum CO_2 content of around 10 000ppm in the gas phase (i.e. around 1%) is necessary to avoid from carbon limitation. Please note however that this is related to gas-liquid mass transfer performance of the PBR. It must be recalled that the total gas flow rate was kept constant for all our experiments, leading to similar mass transfer coefficient ($k_L a$). So those results cannot be extrapolated to other aerating conditions and PBR geometries. A relation between growth and DIC concentration C_T , which is the overall result of carbon fluxes, is more representative (Table 5).

A significantly higher DIC concentration was obtained in Case 5 (>7.1mM), where pure CO_2 was automatically injected from pH regulation. This was in accordance with the aim to achieve non

carbon limiting growth conditions. For all other cases, DIC concentration was found below 1mM, with a decrease related to biomass productivity, as already observed previously for batch culture. This tends to emphasize a growth limitation by the carbon source for DIC value lower than 0.5-1mM, with then a significant and rapid decrease of the resulting growth rate.

Those results can be discussed in regards to carbon concentration mechanisms occurring in microalgae cells. Those mechanisms are indeed known to limit the effect of carbon limitation on growth, by concentrating the intracellular concentration of dissolved carbon to maintain Rubisco activity (Spalding, 2008). Our results tends to emphasize that at macroscopic level, this mainly results in a decrease of growth kinetics. There were indeed no relevant variation in cells biochemical composition, except for the pigment content but which could be accounted for the variation in light attenuation conditions, as a consequence of biomass concentration and growth kinetics decrease.

5 Conclusion

A fully-controlled PBR was developed to determine the carbon fluxes involved in microalgal growth. This set-up was based on the monitoring of both liquid (including biomass) and gaseous phases. Calculation of the carbon recovery percentage based on a complete carbon mass balance demonstrated the accuracy of the measurements obtained. The set-up was then used to characterize gas-liquid mass transfer in the PBR for different operating conditions, such as (i) CO₂ absorption during a CO₂ pulse, and (ii) DIC desorption during N₂ bubbling and without pH regulation. The results were compared to a carbon transfer model, allowing carbon fluxes in the process to be accurately predicted.

Investigations were then extended to the case of *Chlorella vulgaris* growth. Although the same operating conditions were applied, the gas-liquid mass transfer coefficient was found to be affected by the presence of cells, emphasizing the interest of online determination of the k_{1a} value for accurate determination of the carbon fluxes involved in the process.

Differing carbon enrichment of the injected gas phase was then tested, in both and continuous cultures. As expected, an increase in biomass productivity was observed by increasing the CO₂ content of the injected gas. When expressed on a C-mol basis, biomass growth rate was found to be directly related to the gas-liquid mass transfer rate. In all conditions ($y_{CO_2}^i < 7700$ ppm), DIC concentration

remained low (<0.4 mM), resulting definitively in growth limitation by the carbon source. A detailed analysis revealed a growth limitation by the carbon source for DIC value lower than 0.5-1mM. However, no significant effect on the biological CO₂ consumption yield was observed ($Y_{CO_2} = 1.7 - 1.8$ kg CO₂ per kg of biomass), emphasizing the efficiency of carbon concentration mechanisms (CCM) in reducing the limitation effects of the carbon source on the overall metabolism. We also noted that a decrease in total pigment content was obtained when carbon limitation was increased (in both batch and continuous cultures), which also indicated possible metabolism regulation by the light absorption capacity of microalgal cells when the growth rate is reduced by carbon limitation. Possible interaction between the dissolved carbon availability and the light supply can therefore be expected.

Our study demonstrates the overall interest of monitoring the carbon fluxes involved in microalgal culture to understand the correlation between gas-liquid mass transfer, DIC availability and the resulting microalgae growth. The strong relation between these factors is emphasized here. CO₂ removal from the gas phase was also found to be limited (around 50%) even in the case of moderate CO₂ gas phase enrichment (< 7000 ppm), emphasizing that flue gas purification (> 10% in CO₂ in general) using microalgae could be challenging.

In future studies, our modeling approach will be extended to investigate various strategies for optimizing carbon use and fixation in microalgae cultivation systems.

6 Acknowledgements

This work has been sponsored by the French government research program “Investissements d’avenir” through the IMobS³ Laboratory of Excellence(ANR-10-LABX-16-01).

NOMENCLATURE

a	Exchange interfacial area per unit of culture volume [m^{-1}]
C	Concentration [mol.m^{-3}]
C*	Solubility of CO_2 (given by Henry's law) [mol.m^{-3}]
G	Gas molar flowrate [mol.s^{-1}]
H	Henry's constant [Pa]
K_1, K_2	Dissociation equilibrium constants [mol.kg^{-1} or mol.m^{-3}]
K	Constant for CO_2/DIC conversion [dimensionless]
k_L	Mass transfer coefficient (Eq.19) [m.s^{-1}]
k_{La}	Overall volumetric mass transfer coefficient [s^{-1} or h^{-1}]
M	Molar mass for species i [kg.mol^{-1}]
N	Molar flux density between liquid and gaseous phases [$\text{mol.m}^{-2}.\text{s}^{-1}$]
p	Partial pressure [Pa]
P_r	Total pressure [Pa]
$\langle r \rangle$	Volumetrical rate, expressed in mole [$\text{mol.m}^{-3}.\text{s}^{-1}$]
$\langle r' \rangle$	Volumetrical rate, expressed in mass [$\text{kg.m}^{-3}.\text{s}^{-1}$]
t	Time [s]
T	Temperature [K]
V_L	Liquid volume [m^3]
y	Molar fraction in gas phase
Y_{CO_2}	Yield of biological consumption of CO_2

Greek letters

η	CO_2 removal ratio
τ_p	Residence time ($=1/D$, with D the dilution rate)

Subscripts and superscripts

PF	related to PF model
$y_{CO_2}^o$	when used in superscript, related to a reference to output mole fraction (Eq.31)
$y_{CO_2}^i$	when used in superscript, related to a reference to output mole fraction (Eq.31)
i	related to the input
o	related to the output
T	related to total concentration (DIC concentration)
L	related to liquid phase
X	related to biomass
G	related to gas phase

Abbreviations

PBR	Photobioreactor
CRP	Carbon Recovery Percentage

Literature cited

- André, G., Moo-Young, M., Robinson, C.W., 1981. Improved method for the dynamic measurement of mass transfer coefficient for application to solid–substrate fermentation. *Biotechnol. Bioeng.* 23, 1611–1622. <https://doi.org/10.1002/bit.260230718>
- Baba, M., Shiraiwa, Y., 2012. High-response mechanisms in microalgae 588 pages.
- Badger, M.R., Price, G.D., 2003. CO₂ concentrating mechanisms in cyanobacteria: molecular components, their diversity and evolution. *J. Exp. Bot.* 54, 609–622. <https://doi.org/10.1093/jxb/erg076>
- Carlsson, A.S., Van Beilen, J.B., Möller, R., Clayton, D., 2007. Micro- and macro-algae: Utility for industrial applications. cplpress.
- Cheng, L., Zhang, L., Chen, H., Gao, C., 2006. Carbon dioxide removal from air by microalgae cultured in a membrane-photobioreactor. *Sep. Purif. Technol.* 50, 324–329. <https://doi.org/10.1016/j.seppur.2005.12.006>
- Chisti, Y., 2007. Biodiesel from microalgae. *Biotechnol. Adv.* 25, 294–306. <https://doi.org/10.1016/j.biotechadv.2007.02.001>
- Cornet, J.F., Dussap, C., Gros, J.B., 1998. Kinetics and energetics of photosynthetic micro-organisms in photobioreactors, *Bioprocess and Algae Reactor Technology, Apoptosis*, in: *Advances in Biochemical Engineering/Biotechnology*. Springer Berlin / Heidelberg, pp. 153–224. <https://doi.org/10.1007/BFb0102299>
- Degrenne, B., 2009. Production d'hydrogène par *Chlamydomonas reinhardtii* en photobioréacteur: Analyse des conditions de culture et mise en place d'un protocole autotrophe. Université de Nantes.
- Doucha, J., Straka, F., Lívanský, K., 2005. Utilization of flue gas for cultivation of microalgae (*Chlorella* sp.) in an outdoor open thin-layer photobioreactor. *J. Appl. Phycol.* 17, 403–412. <https://doi.org/10.1007/s10811-005-8701-7>
- Edwards, T.J., Newman, J., Prausnitz, J.M., 1975. Thermodynamics of aqueous solutions containing volatile weak electrolytes. *AIChE J.* 21, 248–259. <https://doi.org/10.1002/aic.690210205>
- Fouchard, S., Pruvost, J., Degrenne, B., Legrand, J., 2008. Investigation of H₂ production using the green microalga *Chlamydomonas reinhardtii* in a fully controlled photobioreactor fitted with on-line gas analysis. *Int. J. Hydrog. Energy* 33, 3302–3310. <https://doi.org/10.1016/j.ijhydene.2008.03.067>
- Giordano, M., Beardall, J., Raven, J.A., 2005. CO₂ concentrating mechanisms in algae: mechanisms, environmental modulation, and evolution. *Annu. Rev. Plant Biol.* 56, 99–131.
- Henry, W., 1803. Experiments on the Quantity of Gases Absorbed by Water, at Different Temperatures, and under Different Pressures. *Philos. Trans. R. Soc. Lond.* 93, 29–274.
- Hill, G.A., 2006. Measurement of Overall Volumetric Mass Transfer Coefficients for Carbon Dioxide in a Well-Mixed Reactor Using a pH Probe. *Ind. Eng. Chem. Res.* 45, 5796–5800. <https://doi.org/10.1021/ie060242t>
- Huntley, M., Redalje, D., 2007. CO₂ Mitigation and Renewable Oil from Photosynthetic Microbes: A New Appraisal. *Mitig. Adapt. Strateg. Glob. Change* 12, 573–608. <https://doi.org/10.1007/s11027-006-7304-1>
- Kandilian, R., Soulies, A., Pruvost, J., Rousseau, B., Legrand, J., Pilon, L., 2016. Simple method for measuring the spectral absorption cross-section of microalgae. *Chem. Eng. Sci.* 146, 357–368. <https://doi.org/10.1016/j.ces.2016.02.039>
- Kanniche, M., Gros-Bonnivard, R., Jaud, P., Valle-Marcos, J., Amann, J.-M., Bouallou, C., 2010. Pre-combustion, post-combustion and oxy-combustion in thermal power plant for CO₂ capture. *Appl. Therm. Eng.* 30, 53–62. <https://doi.org/10.1016/j.applthermaleng.2009.05.005>
- Kordac, M., Linek, V., 2008. Dynamic Measurement of Carbon Dioxide Volumetric Mass Transfer Coefficient in a Well-Mixed Reactor Using a pH Probe: Analysis of the Salt and Supersaturation Effects. *Ind. Eng. Chem. Res.* 47, 1310–1317. <https://doi.org/10.1021/ie0711776>
- Lewis, W.K., Whitman, W.G., 1924. Principles of Gas Absorption. *Ind. Eng. Chem.* 16, 1215–1220. <https://doi.org/10.1021/ie50180a002>
- Loubiere, K., Pruvost, J., Aloui, F., Legrand, J., 2011. Investigations in an external-loop airlift photobioreactor with annular light chambers and swirling flow. *Chem. Eng. Res. Des.* 89, 164–171. <https://doi.org/10.1016/j.cherd.2010.06.001>

- Luis, P., Van Gerven, T., Van der Bruggen, B., 2012. Recent developments in membrane-based technologies for CO₂ capture. *Prog. Energy Combust. Sci.* 38, 419–448. <https://doi.org/10.1016/j.peccs.2012.01.004>
- Martzolff, A., Cahoreau, E., Cogne, G., Peyriga, L., Portais, J.-C., Dechandol, E., Le Grand, F., Massou, S., Gonçalves, O., Pruvost, J., Legrand, J., 2012. Photobioreactor design for isotopic non-stationary ¹³C-metabolic flux analysis (INST ¹³C-MFA) under photoautotrophic conditions. *Biotechnol. Bioeng.* n/a-n/a. <https://doi.org/10.1002/bit.24575>
- Miyachi, S., Iwasaki, I., Shiraiwa, Y., 2003. Historical perspective on microalgal and cyanobacterial acclimation to low- and extremely high-CO₂ conditions. *Photosynth. Res.* 77, 139–153. <https://doi.org/10.1023/a:1025817616865>
- Pottier, L., Pruvost, J., Deremetz, J., Cornet, J.F., Legrand, J., Dussap, C.G., 2005. A fully predictive model for one-dimensional light attenuation by *Chlamydomonas reinhardtii* in a torus photobioreactor. *Biotechnol. Bioeng.* 91, 569–582. <https://doi.org/10.1002/bit.20475>
- Price, G.D., Howitt, S.M., 2011. The cyanobacterial bicarbonate transporter BicA: its physiological role and the implications of structural similarities with human SLC26 transporters This paper is one of a selection of papers published in a Special Issue entitled CSBMCB 53rd Annual Meeting — Membrane Proteins in Health and Disease, and has undergone the Journal's usual peer review process. *Biochem. Cell Biol.* 89, 178–188. <https://doi.org/10.1139/O10-136>
- Price, G.D., Sültemeyer, D., Klughammer, B., Ludwig, M., Badger, M.R., 1998. The functioning of the CO₂ concentrating mechanism in several cyanobacterial strains: a review of general physiological characteristics, genes, proteins, and recent advances. *Can. J. Bot.* 76, 973–1002. <https://doi.org/10.1139/b98-081>
- Pruvost, J., Cornet, J.F., Goetz, V., Legrand, J., 2012. Theoretical investigation of biomass productivities achievable in solar rectangular photobioreactors for the cyanobacterium *Arthrospira platensis*. *Biotechnol. Prog.* 28, 699–714. <https://doi.org/10.1002/btpr.1540>
- Pruvost, J., Pottier, L., Legrand, J., 2006. Numerical investigation of hydrodynamic and mixing conditions in a torus photobioreactor. *Chem. Eng. Sci.* 61, 4476–4489. <https://doi.org/10.1016/j.ces.2006.02.027>
- Pruvost, J., Vooren, G.V., Cogne, G., Legrand, J., 2009. Investigation of biomass and lipids production with *Neochloris oleoabundans* in photobioreactor. *Bioresour. Technol.* 100, 5988–5995. <https://doi.org/10.1016/j.biortech.2009.06.004>
- Pulz, O., Gross, W., 2004. Valuable products from biotechnology of microalgae. *Appl. Microbiol. Biotechnol.* 65, 635–648. <https://doi.org/10.1007/s00253-004-1647-x>
- Rice, K.C., Herman, J.S., 2012. Acidification of Earth: An assessment across mechanisms and scales. *Appl. Geochem.* 27, 1–14. <https://doi.org/10.1016/j.apgeochem.2011.09.001>
- Ritchie, R., 2008. Universal chlorophyll equations for estimating chlorophylls *a*, *b*, *c*, and *d* and total chlorophylls in natural assemblages of photosynthetic organisms using acetone, methanol, or ethanol solvents. *Photosynthetica* 46, 115–126. <https://doi.org/10.1007/s11099-008-0019-7>
- Ritchie, R., 2006. Consistent Sets of Spectrophotometric Chlorophyll Equations for Acetone, Methanol and Ethanol Solvents. *Photosynth. Res.* 89, 27–41. <https://doi.org/10.1007/s11120-006-9065-9>
- Roustan, M., 2003. Transferts gaz-liquide dans les procédés de traitement des eaux et des effluents gazeux, Edition TEC&DOC. ed.
- Royce, P.N.C., Thornhill, N.F., 1991. Estimation of dissolved carbon dioxide concentrations in aerobic fermentations. *AIChE J.* 37, 1680–1686. <https://doi.org/10.1002/aic.690371111>
- Solomon, S., Qin, D., Manning, M., Chen, Z., Marquis, M., Averyt, K.B., Tignor, M., Miller, H.L., 2007. Contribution of Working Group I to the Fourth Assessment Report of the Intergovernmental Panel on Climate Change, 2007.
- Souliès, A., Legrand, J., Marec, H., Pruvost, J., Castelain, C., Burghilea, T., Cornet, J.-F., 2016a. Investigation and modeling of the effects of light spectrum and incident angle on the growth of *Chlorella vulgaris* in photobioreactors. *Biotechnol. Prog.* 32, 247–261. <https://doi.org/10.1002/btpr.2244>
- Souliès, A., Legrand, J., Marec, H., Pruvost, J., Castelain, C., Burghilea, T., Cornet, J.-F., 2016b. Investigation and modeling of the effects of light spectrum and incident angle on the growth of *Chlorella vulgaris* in photobioreactors. *Biotechnol. Prog.* 32, 247–261. <https://doi.org/10.1002/btpr.2244>
- Souliès, A., Legrand, J., Marec, H., Pruvost, J., Castelain, C., Burghilea, T., Cornet, J.-F., 2016c. Investigation and modeling of the effects of light spectrum and incident angle on the growth of

- Chlorella vulgaris* in photobioreactors. *Biotechnol. Prog.* 32, 247–261.
<https://doi.org/10.1002/btpr.2244>
- Spalding, M.H., 2008. Microalgal carbon-dioxide-concentrating mechanisms: *Chlamydomonas* inorganic carbon transporters. *J. Exp. Bot.* 59, 1463–1473. <https://doi.org/10.1093/jxb/erm128>
- Strickland, J.D.H., Parsons, T.R., 1968. *A Practical Handbook of Seawater Analysis*. Fisheries Research Board of Canada.
- Takache, H., Pruvost, J., Cornet, J.-F., 2012. Kinetic modeling of the photosynthetic growth of *Chlamydomonas reinhardtii* in a photobioreactor. *Biotechnol. Prog.* 28, 681–692.
<https://doi.org/10.1002/btpr.1545>

Legend of Tables

Table 1: Definitions of carbon flux (gas-liquid mass transfer)

Table 2: Volumetric mass-transfer coefficients obtained for the various absorption-desorption experiments

Table 3: Prediction errors for the three representations of driving force in the mass-transfer model

Table 4: Experimental results for the three batch cultures of *Chlorella vulgaris* grown with varying CO₂ concentration in the injected gas

Table 5: Experimental results for the five continuous cultures of *Chlorella vulgaris* grown with varying CO₂ concentration in the injected gas ($\langle r'_x \rangle_{\max}$ indicates the maximal productivity for a given light and CO₂ enrichment which should be achieved at optimal residence time; $\langle r'_x \rangle_{\text{photolimitation}}$ indicates the maximal productivity obtained without limitation by the carbon source for same light conditions and at optimal residence time)

List of figure captions

Figure 1: Scheme of the lab-scale pilot used to investigate CO₂ assimilation by microalgae.

Figure 2: Determination of k_{LA} value for the carbon desorption experiment in growth medium, as obtained from liquid (a) and gas (b) phase time monitoring. Figures c and d give the Carbon Recovery Percentage (CRP) and linearization procedure for obtaining k_{LA} values for the different definitions of driving force (see Table 1)

Figure 3: Experimental results (blue curve) and model predictions (plug flow model, red curves) of CO₂ absorption in the culture medium with carbon pulse at fixed pH (7.5). Model predictions are given in the form of envelopes (dashed lines), by introducing the possible deviation of experimental operating parameters (i.e. ± 0.1 , $\pm 10^{-4}$ and $\pm 0.2\text{h}^{-1}$ for pH, $y_{CO_2}^i$ and k_{LA} values respectively) to the input parameters of the model. The final averaged model prediction error for C_T is 3.5% and 5.7% for $y_{CO_2}^o$.

Figure 4: Experimental results (blue curve) and model predictions (plug flow model, red curves) of carbon desorption without pH regulation. Model predictions are given in the form of envelopes (dashed lines), by introducing the possible deviation of experimental operating

parameters (i.e. ± 0.1 , $\pm 10^{-4}$ and $\pm 0.2\text{h}^{-1}$ for pH, $y_{CO_2}^i$ and k_{La} values respectively) to the input parameters of the model. The final averaged model prediction errors are 9.8% and 4.5% for C_T and pH respectively (since $y_{CO_2}^o$ values tend to 0, no relative error is given for this quantity).

Figure 5: Time evolutions of biomass and pigment concentrations for experiments E1 and E2 (triangles and circles are for experiments E1 and E2 respectively; full and empty symbols are for biomass and pigments concentrations respectively).

Figure 6: Biomass concentration and corresponding productivities obtained in continuous culture for experiments C1 (400ppm, ●), C2 (2200ppm, ■), C3 (7400ppm, ▲), C4 (9214ppm, —) and C5 (photolimitation condition, ◆); full and empty symbols are for biomass concentration and productivities respectively.

Figure 1

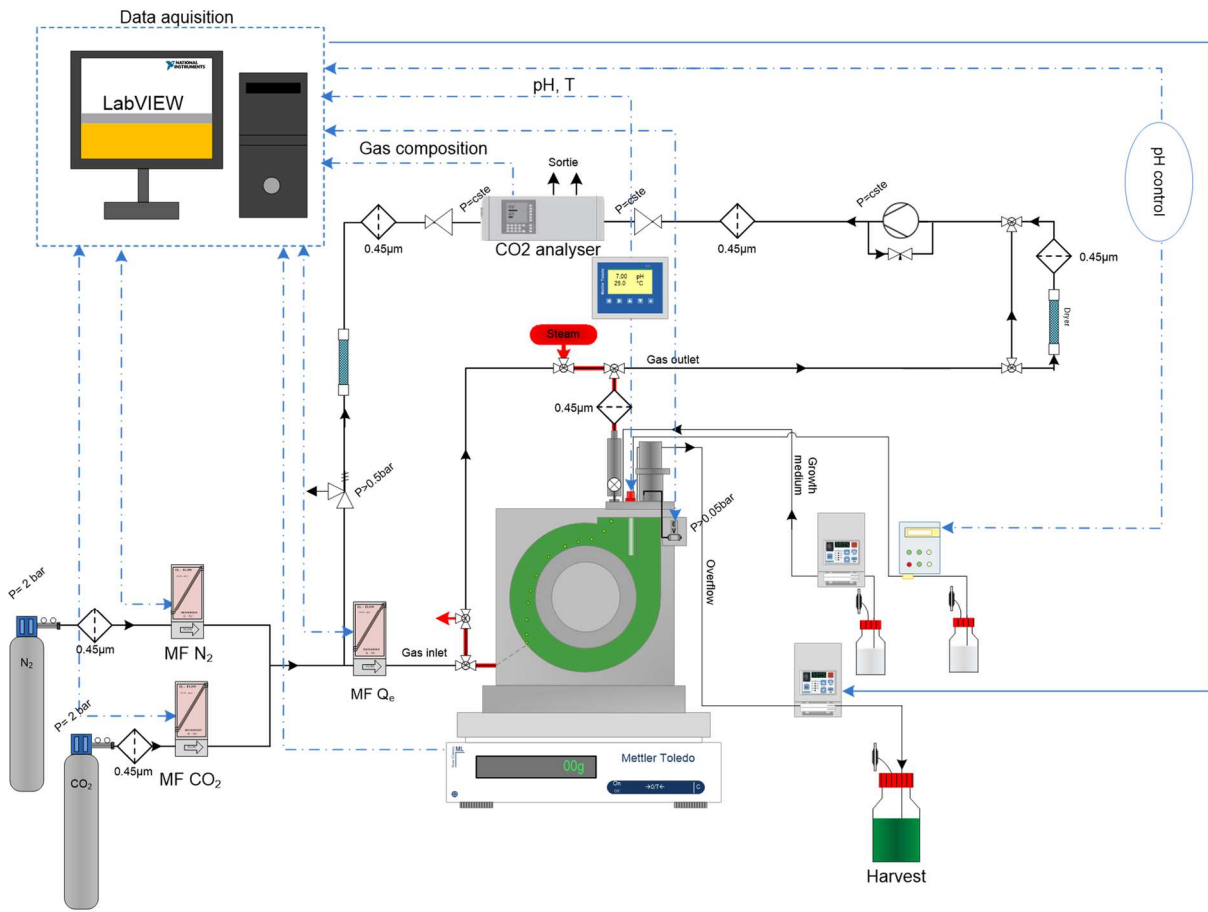


Figure 2

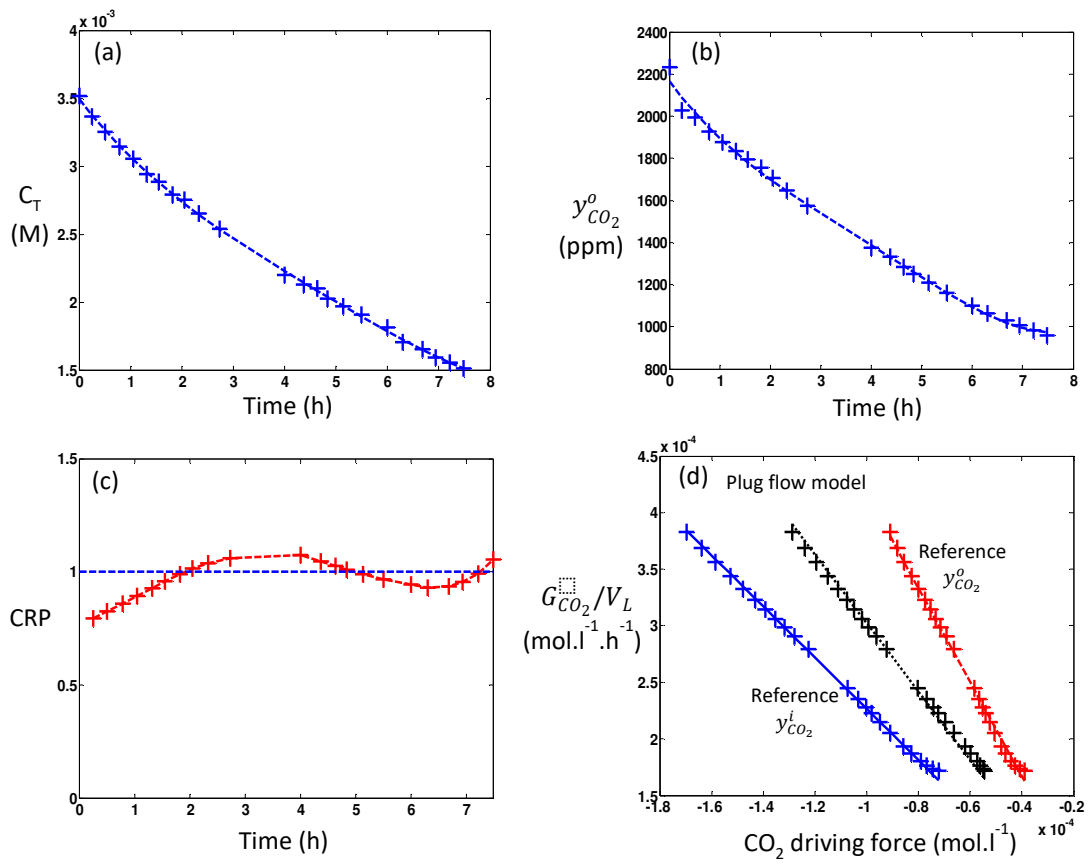


Figure 3

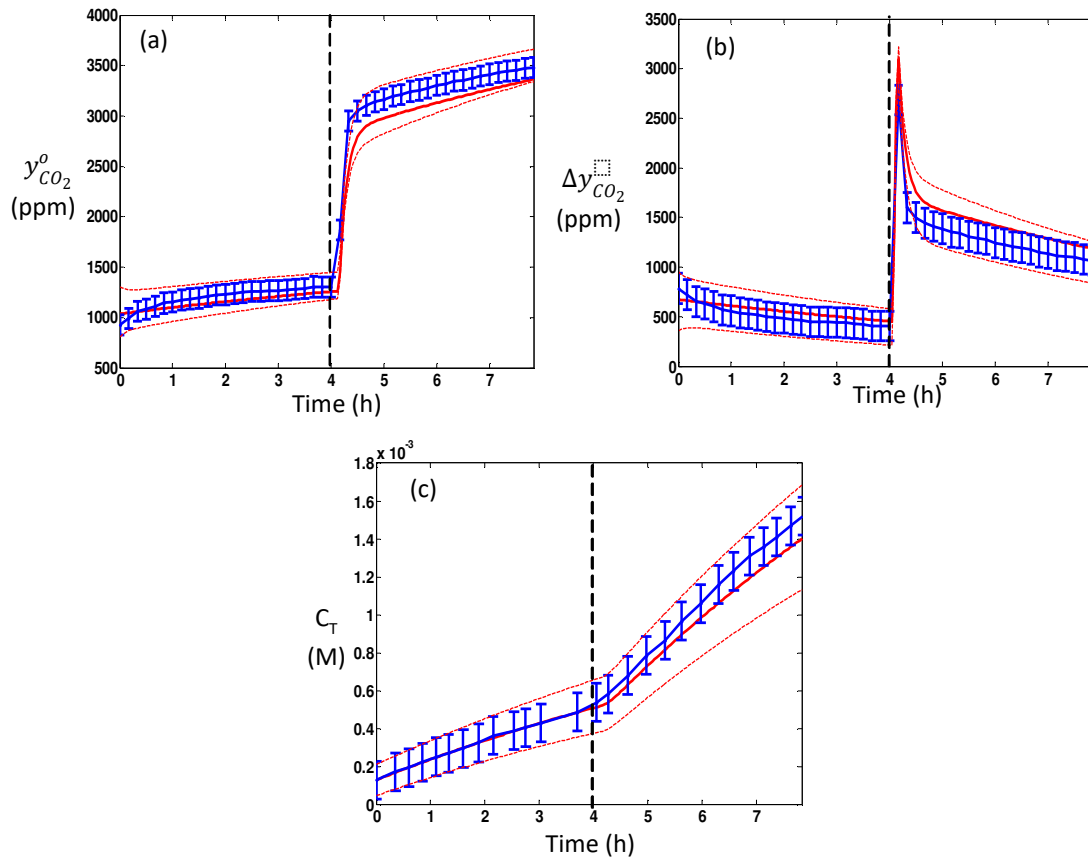


Figure 4

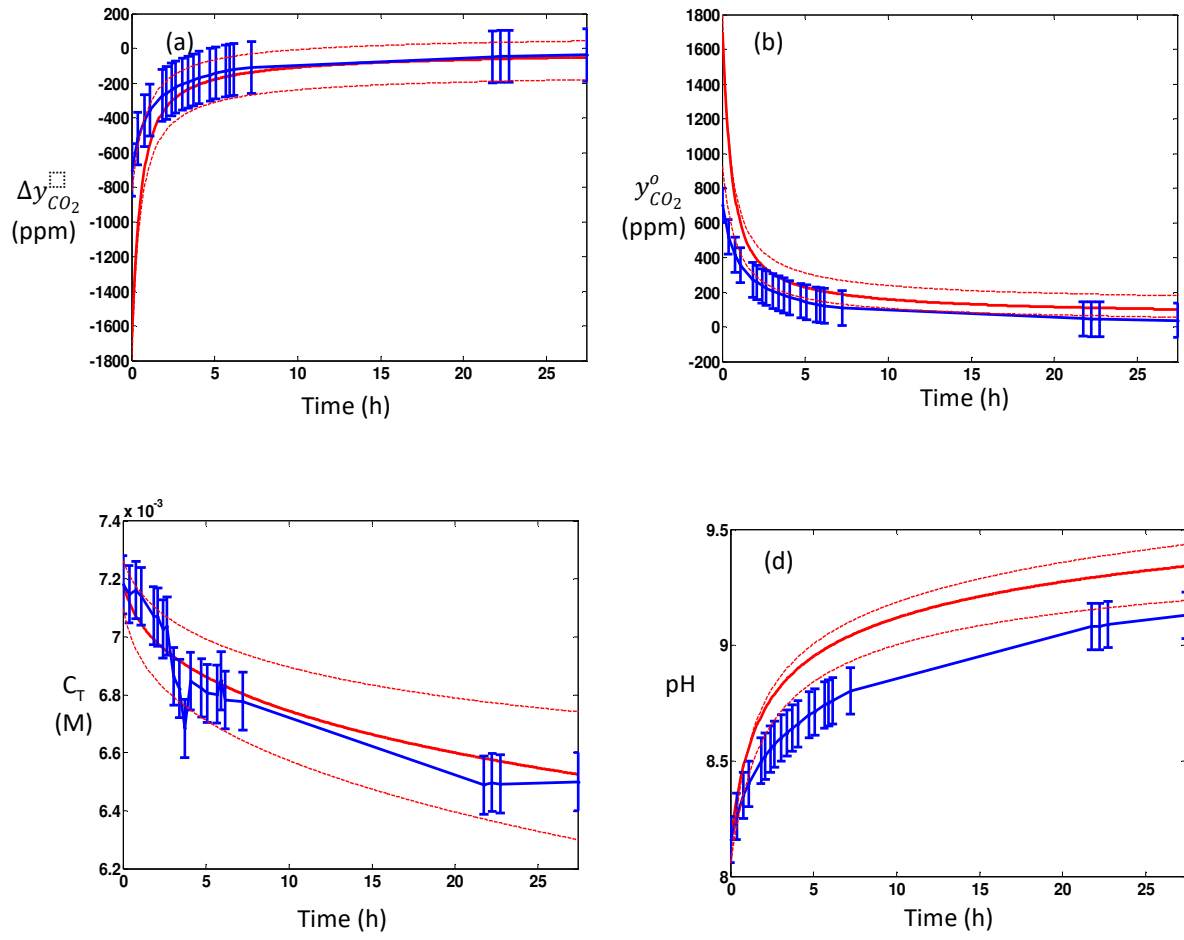


Figure 5

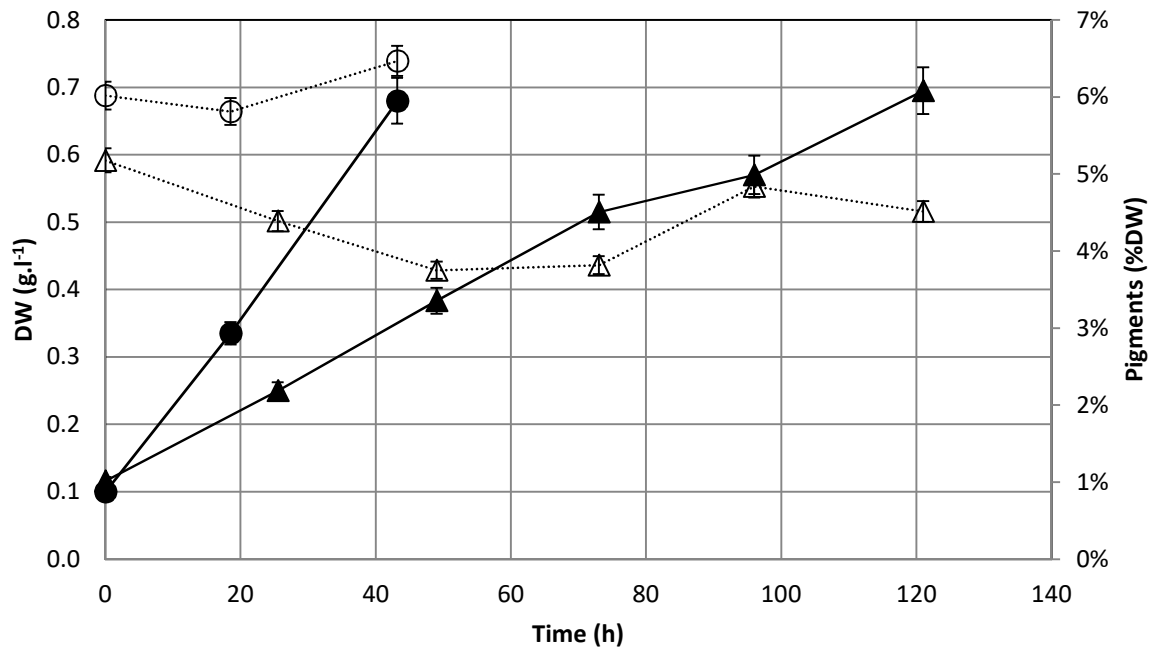


Figure 6

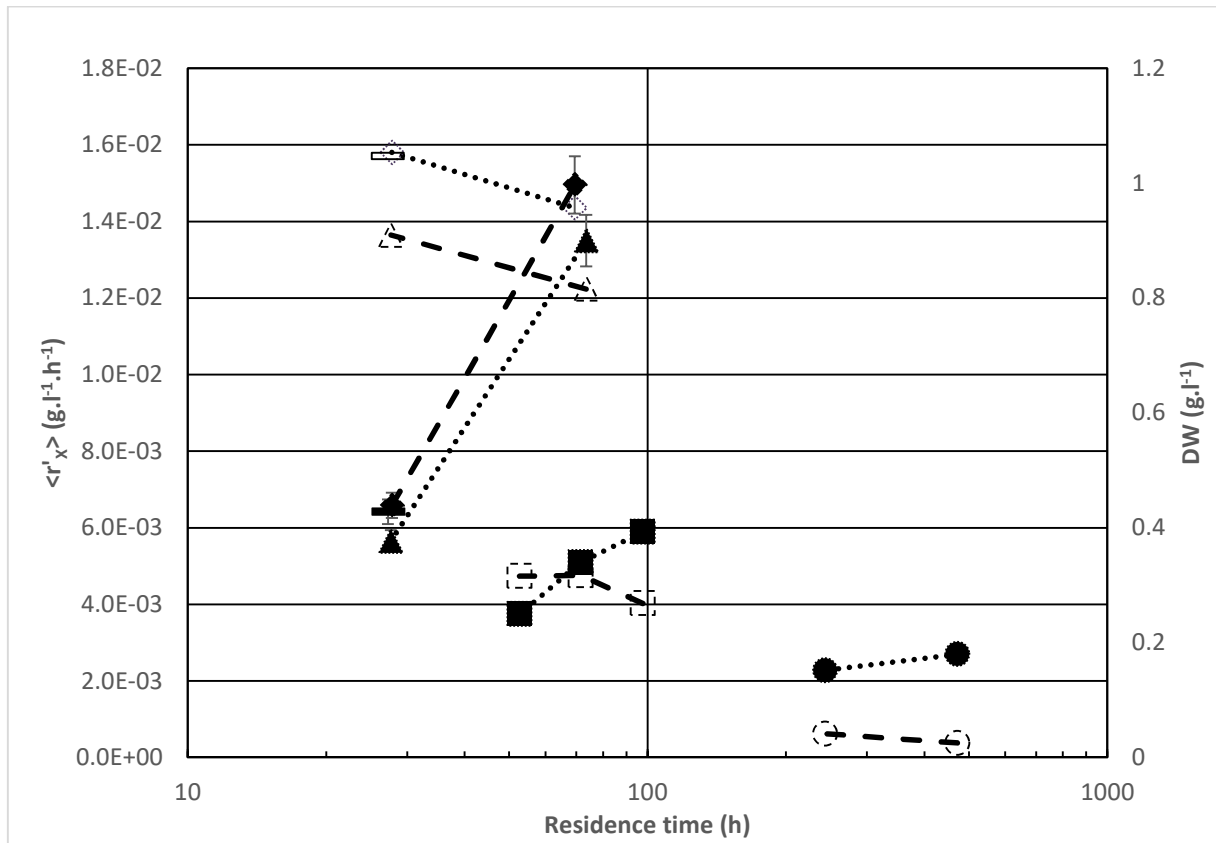


Table 1

Volumetric mass transfer carbon flux definition	
<p>$y_{CO_2}^o$ as reference for well-mixed gas phase (CO₂ in gas outlet)</p>	$a \cdot N_{CO_2} = k_L a^{y_{CO_2}^o} \cdot \left(\frac{y_{CO_2}^o \cdot P}{H} - \frac{C_T}{K} \right)$
<p>$y_{CO_2}^i$ as reference for well-mixed gas phase (CO₂ in gas inlet)</p>	$a \cdot N_{CO_2} = k_L a^{y_{CO_2}^i} \cdot \left(\frac{y_{CO_2}^i \cdot P}{H} - \frac{C_T}{K} \right)$
<p>Plug flow model for gas phase</p>	$a \cdot N_{CO_2} = k_L a^{PF} \frac{\left(\frac{y_{CO_2}^i \cdot P}{H_{CO_2}} - \frac{C_T}{K} \right) - \left(\frac{y_{CO_2}^o \cdot P}{H_{CO_2}} - \frac{C_T}{K} \right)}{\ln \left[\frac{\left(\frac{y_{CO_2}^i \cdot P}{H_{CO_2}} - \frac{C_T}{K} \right)}{\left(\frac{y_{CO_2}^o \cdot P}{H_{CO_2}} - \frac{C_T}{K} \right)} \right]}$

Table 2

Volumetric mass- transfer coefficient (h^{-1})	Carbon absorption experiment		Carbon desorption experiment	
	Sueoka culture medium	De-ionized water	Sueoka culture medium	De-ionized water
$k_L a^{y_{CO_2}^i}$	1.7 ± 0.1	2.0 ± 0.1	2.3 ± 0.1	1.7 ± 0.1
$k_L a^{y_{CO_2}^o}$	2.7 ± 0.1	3.5 ± 0.2	4.1 ± 0.2	2.7 ± 0.1
$k_L a^{PF}$	2.1 ± 0.1	2.6 ± 0.1	3.0 ± 0.2	2.1 ± 0.1
CRP	0.96	0.89	0.97	1.07

Table 3

	Plug flow model	$y_{CO_2}^i$ as reference	$y_{CO_2}^o$ as reference
$k_L a$ value (h^{-1})	2.6±0.1	2.0±0.1	3.5±0.2
Error of prediction C_T	3.5%	2.6%	4.0%
Error of prediction y_s	5.7%	6.4%	5.4%

Table 4

	Incident PFD ($\mu\text{mol}_{\text{hv}} \cdot \text{m}^{-2} \cdot \text{s}^{-1}$)	$y_{\text{CO}_2}^i$ (ppm)	Δy_{CO_2} (ppm)	C_T (mM)	N_{CO_2} ($\text{mol}_c \cdot \text{L}^{-1} \cdot \text{h}^{-1}$)	$\langle r'_x \rangle$ ($\text{g} \cdot \text{L}^{-1} \cdot \text{h}^{-1}$)	$\langle r_x \rangle$ ($\text{mol}_c \cdot \text{L}^{-1} \cdot \text{h}^{-1}$)	Pigment content (%DW)		
								Chl a	Chl b	Total carotenoids
E 1	250	2200	1146	0.02	$1.95 \cdot 10^{-4}$	$(4.75 \pm 0.3) \cdot 10^{-3}$	$(1.98 \pm 0.2) \cdot 10^{-4}$	3.1	0.8	0.8
E 2	250	6500	3610	0.06	$6.14 \cdot 10^{-4}$	$(13.5 \pm 0.9) \cdot 10^{-3}$	$(5.63 \pm 0.4) \cdot 10^{-4}$	4.1	1	1
E 3	400	7700	4030	0.37	$6.82 \cdot 10^{-4}$	$(14.8 \pm 1) \cdot 10^{-3}$	$(6.17 \pm 0.6) \cdot 10^{-3}$	3.5	0.9	0.8

Table 5:

	$y_{CO_2}^i$ (ppm)	Δy_{CO_2} (ppm)	C_T (mM)	N_{CO_2} ($\text{mol}_C \cdot \text{L}^{-1} \cdot \text{h}^{-1}$)	$\langle r'_x \rangle_{\text{max}}$ assumed ($\text{g} \cdot \text{L}^{-1} \cdot \text{h}^{-1}$)	$\langle r'_x \rangle_{\text{max}} /$ $\langle r'_x \rangle_{\text{photolimitation}}$ (%)	Pigment content (%DW)		
							Chl a	Chl b	Total carotenoids
C1	400	200	--	-	$6.00 \cdot 10^{-4}$	3.8	--	--	--
C2	2200	1236	0.02	$2.1 \cdot 10^{-4}$	$4.97 \cdot 10^{-3}$	31.0	2.9	0.6	0.7
C3	7740	3665	0.13	$6.23 \cdot 10^{-4}$	$1.36 \cdot 10^{-2}$	85	4.7	1.2	1.1
C4	9214	4276	0.42	$7.27 \cdot 10^{-4}$	$1.57 \cdot 10^{-2}$	98.1	4.5	1.1	1
C5	Carbon in excess	--	11.42	-	$1.60 \cdot 10^{-2}$	100	3.8	1.0	0.9